Comprehensive numerical simulation of defect density and temperature-dependent transport properties in hydrogenated amorphous silicon

F. Wang
Italian National Institute for Physics of Matter, Research Unit at the Department of Experimental Physics, University of Turin, I-10125 Torino, Italy
and Physics Department E16, Technical University of Munich, D-85747 Garching, Germany

R. Schwarz
Physics Department E16, Technical University of Munich, D-85747 Garching, Germany
(Received 1 May 1995; revised manuscript received 21 August 1995)

In this work the mobility-lifetime products of electrons and holes, $(\mu\tau)_e$ and $(\mu\tau)_h$, the response time of the photocurrent τ_R and the electron drift mobility μ_{de} have been numerically simulated as a function of the dangling bond density N_d and temperature T in hydrogenated amorphous silicon. We have considered all possible recombination and reemission processes occurring between extended and localized states. The simulated results are in good agreement with experimental data. $(\mu\tau)_h$ in undoped *a*-Si:H is insensitive to N_d in the low-N_d range in contrast to $(\mu\tau)_e$. This asymmetric N_d dependence of $(\mu\tau)_e$ and $(\mu\tau)_h$ is attributed to the inherent asymmetry of the density-of-states distribution of the conduction- and valence-band tails. The $\mu\tau$ products and τ_R decrease with the generation rate, whereas μ_{de} increases. The effect of thermal broadening of the band-tail states must be taken into account in the simulation, especially the increase of the characteristic energy of the conduction band-tail states with T. Apart from the defect states, the band-tail states play a very important role in the determination of the photocarrier lifetimes. In the low-N_d range, recombination via the band-tail states dominates over that via dangling bonds, while dangling bonds become the predominant recombination centers in the high-N_d range. The transition from the tail-state-dominated to the defect-state-dominated recombination process depends essentially on the defect density, the temperature, the generation rate, and the Fermi-level position.

I. INTRODUCTION

In the last two decades detailed studies have been performed to investigate the transport properties of hydrogenated amorphous silicon (*a*-Si:H)–related materials due to their great potential for photovoltaic and microelectronic device applications. The dangling bonds are believed to be the predominant recombination centers,[1–5] therefore the density of dangling bonds (N_d) should solely determine the recombination lifetimes (τ_e and τ_h) of both photogenerated electrons and holes.[6] However, many experimental results show that N_d is not the only factor which determines the photoconductivity (σ_{pc}) in undoped *a*-Si:H, especially when N_d is low.[7–9] Furthermore, it is found that the mobility-lifetime products of electrons and holes $[(\mu\tau)_e$ and $(\mu\tau)_h]$ show an asymmetric dependence on N_d. Increasing N_d up to about 5×10^{16} cm^{-3} does not significantly change the ambipolar diffusion length (L_{amb}) which is determined by $(\mu\tau)_h$ in undoped *a*-Si:H, whereas σ_{pc}, which is dominated by $(\mu\tau)_e$, is very sensitive to N_d.[10–13] The asymmetric N_d dependence is difficult to be understood in the framework of the defect-dominated recombination mechanism alone. Previously, Sauvain *et al.* suggested that the change of the charged states of the dangling bonds with N_d is responsible for the effect.[11] However, the present authors proposed in an analytical model that recombination via the valence-band-tail states is the reason for it.[12]

Since no concensus for the explanation of the asymmetric behavior has been reached so far, in the present paper we explore the problem using numerical simulation. Simmons and Taylor extended the Shockley-Read-Hall statistics[14] to amorphous semiconductors, which have a continuous distribution of localized states in the band gap,[15] and simulated the photoconductivity in *a*-Si:H-based materials.[16] Since then, numerical simulation has been extensively used to study the transport properties. The first step in numerical simulation is to choose a proper transport mechanism. The multiple-trapping model has been successfully used to explain photocarrier transport at temperatures above 150 K.[6,7,17–23] The second step in modeling is to assume the distribution of the density of states (DOS) in the mobility gap. In the literature there are two extremes of the assumed DOS distributions of *a*-Si:H. In the first extreme, one neglects the dangling-bond states, and only the recombinations in the tail states are considered.[7,16] The reverse occurs in the second extreme; that is, one considers only the defect states as recombination centers.[18–21] But it is well known that both the conduction-band-tail (CBT) and valence-band-tail (VBT) states and defect states actually coexist in *a*-Si:H-based materials. All these localized states may play an important role in the recombination processes. In this paper we present a comprehensive simulation, which includes recombinations in the tails

 ©1995 The American Physical Society

and the defect states.

The structure of the paper is the following: in Sec. II, we describe the model of simulation which is based on Schockley-Read-Hall statistics. We have considered all possible trapping, recombination, and reemission processes which may occur between the extended and localized states in the gap. In Sec. III we simulate $(\mu\tau)_e$ and $(\mu\tau)_h$, then the response time (τ_R) of photocurrent and the electron drift mobility (μ_{de}) as a function of N_d. The simulation reproduces quite well the asymmetric N_d dependence of the $\mu\tau$ products. It shows that the asymmetric N_d dependence of the $\mu\tau$ products is caused by the inherent asymmetry of the DOS distributions of the CBT and VBT states.

A key parameter determining the proper carrier transport mechanism is the temperature (T), because the reemission rate of trapped carriers is strongly dependent on this quantity. Therefore, in order to check the validity of our simulation model, we have also calculated the T dependence of these transport parameters in Sec. IV. In the temperature range from 150 to 450 K, the simulated results are in good agreement with experimental data. In addition, from the comparison of the simulation with experimental results we conclude that the increase of the characteristic energy of the band-tail states with increasing T must be taken into account.

II. THEORY OF THE SIMULATION

A. Model of the DOS structure

Although the real DOS structure in the mobility gap of a-Si:H can be quite complicated, and depends on preparation methods and post-growth treatments, in our simulation we choose the most frequently used DOS structure in the literature as shown in Fig. 1. The extended states of the conduction and valence bands are separated from their respective tail states by their mobility edges E_c and E_v. The DOS distributions for the CBT and VBT states are assumed to be single exponential functions of energy with their respective characteristic energies E_{oc} and E_{ov},

$$N_{ct}(E)=N_{co}e^{-(E_c-E)/E_{oc}}, \quad N_{vt}(E)=N_{vo}e^{-E/E_{ov}}, \qquad (1)$$

where E is the energy level measured from E_v. N_{co} and N_{vo} are the density of states at E_c and E_v, respectively.

The dangling bonds have three possible charge states, namely the negatively charged D^- state in which an additional electron is trapped, the neutral D^0 state which has its own electron, and the positively charged D^+ state in which a hole is trapped. Some researchers have proposed Gaussian functions to describe the distributions of these defect states in energy.[6] However, as will be discussed below, since the peak positions of the defect states are far away from both E_c and E_v and the width is narrow (between 0.2 and 0.4 eV),[24,25] in practice the reemission of trapped carriers from the defect states back to the extended states is negligible. Therefore, we can neglect the detailed energetic distribution of the defect states and use δ functions to represent them. The D^+ and D^0 states are assumed to be at the same energy level as E_d, and the energy level for the D^- states is higher than the D^0 states by a correlation energy U. Table I lists the parameters of the DOS structure in our simulation, which are within the range of published values in the literature.[24–31]

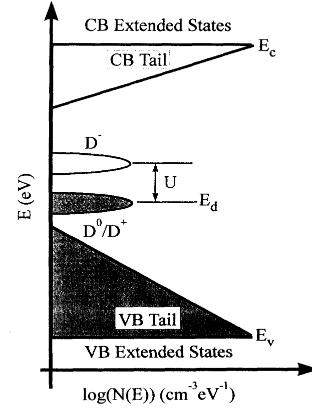

FIG. 1. Model of the density-of-states distribution in the mobility gap used for the simulation.

B. Occupation functions in different gap states

As pointed out by Rose,[32] a carrier trapped in a localized state has the possibility to be thermally reemitted back to its extended state, or to recombine with a carrier of opposite sign. In other words, any localized state can be either a recombination center or a trap state depending on the temperature, on the carrier concentrations, and on its capture cross section and energy level. Therefore, we have considered all the possible recombination and reemission paths which may take place in the tails and the defect states as shown in Fig. 2. Here we neglect the direct recombination between free electrons and holes in the extended states since, under the normal photoexcitation level, both the free-electron and hole densities (n_f and p_f) are much lower than the density of localized states. Hence the indirect recombination via the localized states dominates the carrier recombination process. Furthermore, we neglect the transitions of the carriers

TABLE I. Some parameters of the DOS distribution in the mobility gap.

Parameter	E_g	E_{oc}	E_{ov}	E_d	U	$N_{co}=N_{vo}$	μ_e	μ_h
value	1.9	30	55	0.9	0.3	3×10^{22}	12	3.5
unit	eV	meV	meV	eV	eV	$cm^{-3}\,eV^{-1}$	$cm^2\,V^{-1}\,s^{-1}$	$cm^2\,V^{-1}\,s^{-1}$

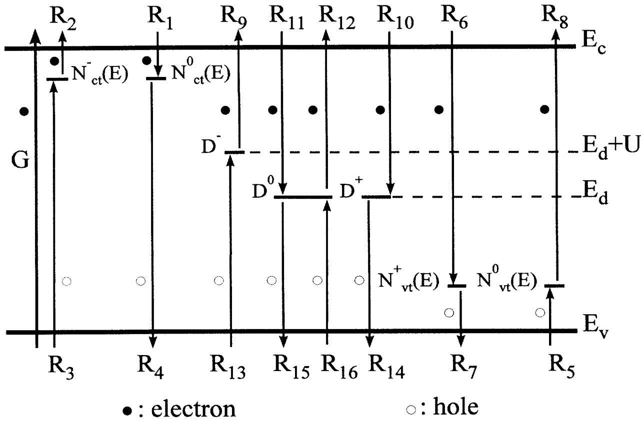

FIG. 2. Recombination and reemission paths considered in the simulation.

among the localized states (tunneling or hopping processes), which may become more important at low temperatures.

Before we calculate the occupation functions in the gap states, we should mention the possible charge states which may exist in the CBT and VBT states. A neutral CBT state can trap an electron and become negatively charged. In reverse, a negatively charged CBT state can return to neutral when it loses its trapped electron due to recombination or reemission. Therefore, the two possible charge states for a CBT state are either neutral or negatively charged. In a similar argument, the VBT states can have either neutral or positively charged states. As discussed above, a defect state has three possible charge states. Next we calculate the occupation functions in the different gap states separately.

As shown in Fig. 2, there are four processes which may take place in a CBT state of energy level E, which are represented by the following four reactions with the rates $R_1(E)$ to $R_4(E)$:

$$N_{ct}^0(E)+e \rightarrow N_{ct}^-(E), \quad R_1(E)=c_1 n_f N_{ct}^0(E) , \tag{2}$$

$$N_{ct}^-(E) \rightarrow N_{ct}^0(E)+e , \quad R_2(E)=\nu e^{-(E_c-E)/k_B T} N_{ct}^-(E) , \tag{3}$$

$$N_{ct}^-(E)+h \rightarrow N_{ct}^0(E), \quad R_3(E)=c_2 p_f N_{ct}^-(E) , \tag{4}$$

$$N_{ct}^0(E) \rightarrow N_{ct}^-(E)+h, \quad R_4(E)=\nu e^{-E/k_B T} N_{ct}^0(E) , \tag{5}$$

where $R_1(E)$ corresponds to the capture of a free electron by a neutral CBT state, $R_2(E)$ is the reemission of a trapped electron back to the conduction band, $R_3(E)$ is the capture of a free hole by a trapped electron and subsequent recombination, and $R_4(E)$ is the thermal excitation of an electron from the valence band into a neutral CBT state (or, in other words, a neutral CBT state emits a hole to the valence band). $N_{ct}^0(E)$ and $N_{ct}^-(E)$ are the density of the neutral and negatively charged CBT states, k_B is the Boltzmann constant, and ν is the attempt-to-escape frequency for trapped carriers. $c_1=v s_{coe}$ (s_{coe} is the capture cross section of neutral CBT states for free electrons, and v is the thermal velocity). $c_2=v s_{cnh}$ (s_{cnh} is the capture cross section of negatively charged CBT states for free holes).

In the steady state, the continuity condition for $N_{ct}^0(E)$ and $N_{ct}^-(E)$ requires

$$\frac{dN_{ct}^0(E)}{dt}=-\frac{dN_{ct}^-(E)}{dt} = R_2(E)+R_3(E)-R_1(E)-R_4(E)=0 . \tag{6}$$

As a result,

$$\nu e^{-(E_c-E)/k_B T} N_{ct}^-(E)+c_2 p_f N_{ct}^-(E) = \nu e^{-E/k_B T} N_{ct}^0(E)+c_1 n_f N_{ct}^0(E) . \tag{7}$$

Since $N_{ct}(E)=N_{ct}^-(E)+N_{ct}^0(E)$, $N_{ct}^-(E)$ can be expressed in terms of $N_{ct}(E)$:

$$N_{ct}^-(E)=\frac{\nu e^{-E/k_B T}+c_1 n_f}{\nu e^{-E/k_B T}+\nu e^{-(E_c-E)/k_B T}+c_1 n_f+c_2 p_f} \times N_{ct}(E) . \tag{8}$$

Finally, the fraction $f_{ct}^-(E)$ of negatively charged CBT states is

$$f_{ct}^-(E)=\frac{N_{ct}^-(E)}{N_{ct}(E)} = \frac{\nu e^{-E/k_B T}+c_1 n_f}{\nu e^{-E/k_B T}+\nu e^{-(E_c-E)/k_B T}+c_1 n_f+c_2 p_f} , \tag{9}$$

As a result, the fraction $f_{ct}^0(E)$ of neutral CBT states is $1-f_{ct}^-(E)$.

In a similar way, the fraction $f_{vt}^+(E)$ of positively charged VBT states is (see Appendix A)

$$f_{vt}^+(E)=\frac{N_{vt}^+(E)}{N_{vt}(E)} = \frac{c_3 p_f+\nu e^{-(E_c-E)/k_B T}}{\nu e^{-E/k_B T}+\nu e^{-(E_c-E)/k_B T}+c_4 n_f+c_3 p_f} , \tag{10}$$

and for neutral VBT states, its fraction $f_{vt}^0(E)$ is $1-f_{vt}^+(E)$.

The fraction $f_d^0(E_d)$ of the D^0 states is (see Appendix B)

$$f_d^0(E_d)=\frac{N_d^0(E_d)}{N_d}=\left[1+\frac{c_8p_f+\nu e^{-(E_c-E_d)/k_BT}}{c_5n_f+\nu e^{-E_d/k_BT}}+\frac{\nu e^{-E_d/k_BT}+c_6n_f}{\nu e^{-(E_c-E_d-U)/k_BT}+c_7p_f}\right]^{-1} . \quad (11)$$

Finally the fractions $[f_d^-(E_d+U)$ and $f_d^+(E_d)]$ of the D^- and D^+ states can be expressed in terms of $f_d^0(E_d)$, respectively,

$$f_d^-(E_d+U)=\frac{N_d^-(E_d+U)}{N_d}=\frac{\nu e^{-E_d/k_BT}+c_6n_f}{\nu e^{-(E_c-E_d-U)/k_BT}+c_7p_f}f_d^0(E_d) , \quad (12)$$

$$f_d^+(E_d)=\frac{N_d^+(E_d)}{N_d}=\frac{c_8p_f+\nu e^{-(E_c-E_d)/k_BT}}{c_5n_f+\nu e^{-E_d/k_BT}}f_d^0(E_d) . \quad (13)$$

In fact, $f_d^0(E_d)$, $f_d^-(E_d+U)$, and $f_d^+(E_d)$ can be further simplified to

$$f_d^0(E_d)=\left[1+\frac{c_8p_f}{c_5n_f}+\frac{c_6n_f}{c_7p_f}\right]^{-1} ,$$
$$f_d^-(E_d+U)=\frac{c_6n_f}{c_7p_f}f_d^0(E_d), \quad f_d^+(E_d)=\frac{c_8p_f}{c_5n_f}f_d^0(E_d) . \quad (14)$$

The conditions for the above simplification are that the reemission terms ($\nu e^{-(E_c-E_d)/k_BT}$, $\nu e^{-E_d/k_BT}$, and $\nu e^{-(E_c-E_d-U)/k_BT}$) are much smaller than the capture terms (c_5n_f, c_6n_f, c_7p_f, and c_8p_f). These conditions can be normally fulfilled as long as E_d and E_d+U are located about 0.6 eV away from both E_c and E_v. For example, if we assume that $n_f=p_f=10^{12}$ cm^{-3}, which corresponds to $\sigma_{\rm pc}$ of about 10^{-6} Ω^{-1}cm^{-1}, then $c_6n_f=5\times10^3$ s^{-1}, but $\nu e^{-E_d/k_BT}=2$ s^{-1} at room temperature when $E_d=0.7$ eV. The significance of the above simplifications is that the fractions of the different charge states are determined only by the coefficients c_5-c_8 and the free-carrier densities, but independent of E_d and U. This is the reason why we can choose δ functions to describe the energy distributions of the defect states in our simulation. Similar simplifications have been used by Hubin, Shah, and Sauvain.[19]

However, the energy range of E_d within which $f_d^0(E_d)$, $f_d^-(E_d+U)$, and $f_d^+(E_d)$ are insensitive to E_d depends strongly on T. In particular, at high temperatures those simplifications are not valid because the reemission terms cannot be neglected. Therefore, in our simulation we still use Eqs. (11)–(13), instead of the simplified forms given by Eq. (14).

From the above discussion we conclude that the occupation functions of the defect states and of the CBT and VBT states are determined by n_f, p_f, and T once the DOS structure and a set of capture cross sections have been chosen. The capture cross sections in our simulation are listed in Table II. We assume the same capture cross section of the charged CBT and VBT states for opposite sign free carriers, which is larger than those of their corresponding neutral states. The same assumption is made for the different defect states.

TABLE II. List of the parameters used for the numerical simulation.

Parameter	v	ν	$s_{coe}=s_{voh}$	$s_{cnh}=s_{vpe}$	$s_{dnh}=s_{dpe}$	$s_{doe}=s_{doh}$
value	10^7	10^{12}	10^{-16}	5×10^{-16}	10^{-15}	5×10^{-16}
unit	cm/s	s^{-1}	cm^2	cm^2	cm^2	cm^2

C. Simulation procedure

Carrier transport in the framework of the multiple-trapping mode is dominated by free carriers. In the simulation the free-electron and hole mobilities at their mobility edges (μ_e and μ_h) are treated as constants. Therefore, the $\mu\tau$ products can be obtained once τ_e and τ_h are calculated.

τ_e and τ_h are related to n_f and p_f and the generation rate g by $n_f=g\tau_e$ and $p_f=g\tau_h$. Then $(\mu\tau)_e=\mu_e n_f/g$ and $(\mu\tau)_h=\mu_h p_f/g$. n_f and p_f can be obtained by solving the following two combined equations (the charge neutrality and rate equations) using numerical iteration.

(a) The charge neutrality equation reads

$$Q_s=n_f-p_f+N_A^--N_D^++\int_0^{E_c}N_{ct}(E)f_{ct}^-(E)dE-\int_0^{E_c}N_{vt}(E)f_{vt}^+(E)dE+N_df_d^-(E_d+U)-N_df_d^+(E_d) , \quad (15)$$

where $-eQ_s$ is the density of the space charge. For a uniform bulk material, Q_s is zero. On the right-hand side of the above equation, N_A^- and N_D^+ are the densities of ionized acceptors and donors, the first integral (the fifth term) is the total density of electrons captured in the CBT states, while the second integral (the sixth term) is the total density of holes captured in the VBT states. The seventh and eighth terms are the densities of electrons and holes captured in the dangling-bond states, respectively.

(b) The rate equation of free electrons and holes in the steady state is

$$\frac{dn_f}{dt}=\frac{dp_f}{dt}=g-R_{\rm tot}=0 , \quad (16)$$

where $R_{\rm tot}$ is the total recombination rate which is the sum of the net recombination rates in the dangling bonds (R_d), in the CBT (R_{ct}), and in the VBT states (R_{vt}). Here R_{ct}, R_{vt}, and R_d have the following forms:

$$R_{ct}=\int_0^{E_c}[R_1(E)-R_2(E)]dE$$
$$=\int_0^{E_c}[R_3(E)-R_4(E)]dE\ , \quad (17)$$
$$R_{vt}=\int_0^{E_c}[R_6(E)-R_8(E)]dE$$
$$=\int_0^{E_c}[R_5(E)-R_7(E)]dE\ , \quad (18)$$
$$R_d=R_{11}(E_d)+R_{10}(E_d)-R_9(E_d+U)-R_{12}(E_d)$$
$$=R_{13}(E_d+U)+R_{16}(E_d)-R_{15}(E_d)-R_{14}(E_d)\ . \quad (19)$$

III. RESULTS AND DISCUSSION

A. Dependence of $\mu\tau$ products on N_d

As a first application of our simulation program we calculated the $\mu\tau$ products as a function of N_d spanning from 10^{15} to 10^{19} cm^{-3} with an activation energy E_a of 0.8 eV (here E_a is defined as E_c-E_f) and at a constant T of 300 K.

Then the calculated results are compared with our experimental data measured from two series of undoped *a*-Si:H samples in which N_d ranges from about 3×10^{15} to 2×10^{18} cm^{-3}. The measured $(\mu\tau)_e$ was evaluated from σ_{pc} using the relation $\sigma_{pc}\approx eg(\mu\tau)_e$, where e is the electron charge. L_{amb} has been measured by means of the steady-state photocarrier grating (SSPG) technique.[33,34] Then $(\mu\tau)_h$ was evaluated from the relation $L_{amb}\approx\sqrt{2k_BT/e(\mu\tau)_h}$. This is valid since $(\mu\tau)_e\gg(\mu\tau)_h$ in undoped *a*-Si:H. The excitation source is a HeNe laser (1.96 eV) and its intensity is 3.4 mW/cm^2, corresponding to a generation rate of about 5×10^{19} cm^{-3}s^{-1}. Such a low intensity does not cause any observable change of the optoelectronic properties during the measurements. N_d was obtained from the constant photocurrent (CPM) spectra.[35]

In the first series of the samples N_d was changed by utilizing the Staebler-Wronski effect;[36] that is, the samples were illuminated under white light with an intensity of 100 mW/cm^2 for different durations. In this case N_d increases up to about 4×10^{16} cm^{-3} when the sample has been illuminated for 80 h. In the second series, N_d was varied by annealing the samples at different temperatures from 200 to 550 °C for 30 min in a nitrogen atmosphere. In this way N_d has been increased up to 3×10^{18} cm^{-3}. The activation energy of the samples was between 0.78 and 0.82 eV, which was deduced from the temperature dependence of the dark conductivity in the temperature range between 200 °C and room temperature. The details about the second series can be found in our previous publication.[12]

Figure 3 shows the calculated results (lines) at two generation rates. The measured $(\mu\tau)_e$ and $(\mu\tau)_h$ are denoted by solid and open symbols (squares: first series; triangles: second series), respectively. The simulated results are in good agreement with experimental data. In this figure the asymmetric N_d dependence of $(\mu\tau)_e$ and $(\mu\tau)_h$ is clearly seen. $(\mu\tau)_h$ behaves quite differently from $(\mu\tau)_e$

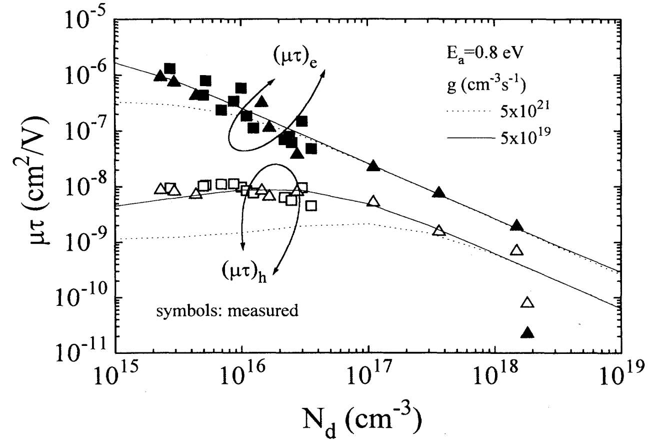

FIG. 3. The $\mu\tau$ products as a function of N_d. The lines are the simulated curves and the symbols (solid: electrons; open: holes) are the measured data. The squares are measured from the light-soaked series, and the triangles are from the high-temperature annealed series.

in the low-N_d range. Take the case of $g=5\times10^{19}$ cm^{-3}s^{-1} as an example. $(\mu\tau)_h$ does not decrease with increasing N_d when $N_d\le3\times10^{16}$ cm^{-3}; it even increases slightly in the very low-N_d range. However, $(\mu\tau)_e$ decreases monotonically with N_d, and can be approximated by a linear function of the inverse of N_d. When N_d is higher than 10^{17} cm^{-3}, both of them show a similar dependence on N_d.

As g increases, both $(\mu\tau)_e$ and $(\mu\tau)_h$ decrease. But the effect of g on the $\mu\tau$ products becomes less pronounced when N_d increases. These results are consistent with the normally observed power-law dependence of σ_{pc} and L_{amb} on light intensity,[11,37,38] namely $\sigma_{pc}\propto g^{\gamma_{pc}}$, and $L_{amb}\propto g^{\gamma_l-1}$, where γ_{pc} and γ_l are the exponents which are less than unity and approach unity with increasing N_d.[12] In the case of $g=5\times10^{21}$ cm^{-3} s^{-1}, $(\mu\tau)_e$ also shows its insensitivity to N_d in the very low-N_d range. Meanwhile, the N_d range within which $(\mu\tau)_h$ is insensitive to N_d is extended.

The distributions of trapped electron and hole densities in the CBT and VBT states have been calculated according to $N_{ct}^-(E)=N_{ct}(E)f_{ct}^-(E)$ and $N_{vt}^+(E)=N_{vt}(E)f_{vt}^+(E)$, respectively. Figure 4 shows two cases with N_d of 3×10^{15} and 3×10^{17} cm^{-3}, respectively. It is clear that there are a lot of carriers trapped in the tail states; their total density and energetic distributions depend on N_d. Let us first discuss the trapped holes. The peak position of $N_{vt}^+(E)$ moves toward midgap when N_d increases. Below the peak, most of the VBT states are neutral, and $f_{vt}^+(E)$ decreases almost exponentially with decreasing E. Above the peak, only a small part of the VBT states are occupied by holes, and $f_{vt}^+(E)$ becomes insensitive to E because in this case the VBT states are so deep that we can neglect the thermal reemission terms in Eq. (10).

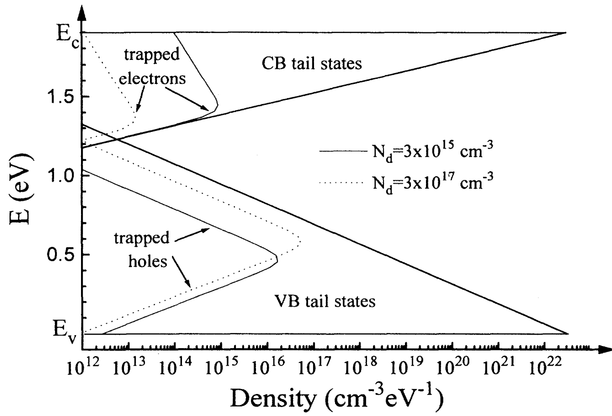

FIG. 4. The distribution of the densities of electrons and holes trapped in the CBT and VBT states for two different values of N_d at $g=5\times10^{19}$ cm^{-3} s^{-1}.

Then

$$f_{vt}^{+}(E)=\frac{c_3p_f}{c_4n_f+c_3p_f} \ . \tag{20}$$

Therefore $f_{vt}^{+}(E)$ is determined only by the ratio of n_f to p_f. This portion of the trapped holes have a very high probability to capture electrons and recombine. Therefore, either for free electrons or holes these deep VBT states will be recombination centers. Similar arguments can be applied to trapped electrons in the CBT states. However, on the one hand the trapped electrons are in much shallower states than the trapped holes. On the other hand, the integrated trapped hole density is much higher than the trapped electron density. Therefore, as will be seen below, the CBT states will play mainly the role of shallow trap states, instead of recombination centers.

It is seen from our simulation that the occupation functions of the defect states change with N_d. For instance, in the case of $g=5\times10^{19}$ cm^{-3} s^{-1}, a large fraction of the defect states are in D^- states when N_d is low. As N_d increases, f_d^- decreases, whereas f_d^0 and f_d^+ increases. As $N_d\geq10^{17}$ cm^{-3} they become saturated, and most of the defect states are in D^0 states. Since D^- states have a larger capture cross section for free holes than D^0 states, the decrease of f_d^- with N_d indicates that the average capture cross section of the defect states for holes becomes small. In contrast, the average capture cross section of the defect states for electrons should increase with N_d. This partially seems to explain the asymmetric N_d dependence of $(\mu\tau)_e$ and $(\mu\tau)_h$.

As already discussed, recombination can take place in all the CBT, VBT, and defect states. Therefore, to clarify which recombination path is more important, one should compare R_{vt}, R_{ct}, and R_d. R_{ct}, according to Eq. (17), is negligible when compared to the other two paths. Therefore, we just compare R_{vt} and R_d calculated from Eqs. (18) and (19). Figure 5 shows the ratio of R_{vt} to R_d as a function of N_d at two generation rates. It is found that recombination via defect states is not the predominant process at low N_d. In the case of $g=5\times10^{19}$ cm^{-3} s^{-1} and $N_d=10^{15}$ cm^{-3}, R_{vt} is about two orders of magnitude higher than R_d. The simple reason is that in the VBT states the density of trapped holes, which are available as recombination centers for electrons, is higher than N_d. When $N_d\geq3\times10^{16}$ cm^{-3} (roughly corresponding to the N_d value above which the asymmetric N_d dependence of the $\mu\tau$ products disappears), R_d becomes larger than R_{vt}. In this case the deep VBT states available as recombination centers are less than N_d. Increasing g extends the N_d range in which recombination in the VBT states dominates.

We should go further to explore the origin of the asymmetric N_d dependence from the DOS structure of a-Si:H. We have recalculated $(\mu\tau)_e$ and $(\mu\tau)_h$ as functions of N_d by assuming an unrealistic DOS structure in the gap, namely $E_{oc}=E_{ov}$. The results are shown in Fig. 6. As one can see, when the DOS structures of the CBT and VBT states are the same, the asymmetric N_d dependence disappears. $(\mu\tau)_h$ changes parallel with $(\mu\tau)_e$. When E_{oc} (E_{ov}) is large, both of them are insensitive to N_d when N_d is low because the recombination in the tail states dominates. In return, when E_{oc} (E_{ov}) is small, both of them are very sensitive to N_d in the whole range of N_d. Now it is clear that in the low-N_d range the asymmetric N_d dependence of the $\mu\tau$ products in undoped a-Si:H samples is caused by the inherent asymmetry of the DOS structures of the CBT and VBT states. The recombination through the tail states plays a critical role for this effect.

The good agreement between the simulated and the measured $\mu\tau$ products encourages us to calculate the

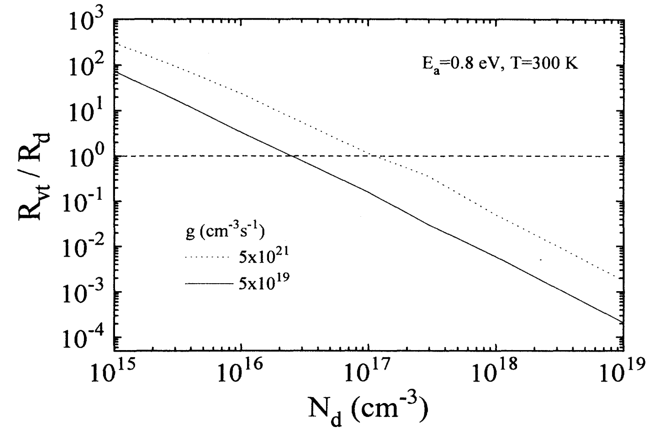

FIG. 5. The ratio of the net recombination rate via the VBT states to that via the defect states for two different values of g. The horizontal line separates the defect-dominated recombination region (lower) from the valence-band-tail-dominated recombination region (upper).

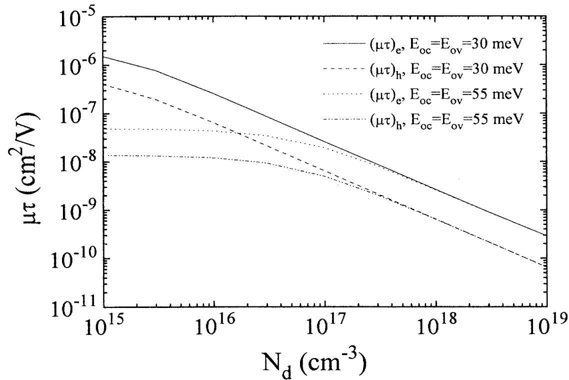

FIG. 6. The simulated $\mu\tau$ products as a function of N_d under the assumption that $E_{oc}=E_{ov}$. It clearly shows that the asymmetric N_d dependence disappears in this case.

response time of the photocurrent and the electron drift mobility further. Due to the continuous distribution of trap states in the gap, generally the transient photocurrent cannot be described by a single exponential function of time.[39,40] Therefore, τ_R is usually taken from the initial decay of the transient current.[39,41] It is also possible to obtain a single exponential decay of photocurrent when one applies a strong dc bias light during the transient measurement.[38,42,43]

When electrons dominate the photocurrent, τ_R is related to τ_e by[32]

$$\tau_R=\frac{N_t+n_f}{n_f}\tau_e \ . \tag{21}$$

Here we should emphasize that N_t is the density of the electrons trapped in the shallow trap states. The electrons captured by deep states no longer contribute to the conduction because there is only a very small possibility that they will be thermally reemitted back to the extended states before recombination. According to Rose's argument a demarcation level E_{de} can be introduced for the conduction-band-tail states by equating the thermal reemission $[R_2(E)]$ and the recombination $[R_3(E)]$ terms. The states above E_{de} have a much higher probability to be reemitted back; therefore, they can be treated as trap states. In reverse, the states below E_{de} are recombination centers. Under our light intensity p_f is between 10^9 and 10^{12} cm^{-3}; therefore, at room temperature E_{de} is located between about 0.68 and 0.50 eV below E_c. This means that most of the CBT states can be treated as trap states. Therefore, N_t can be obtained approximately by integrating the trapped electron density in the CBT states,

$$N_t=\int_0^{E_c}N_{ct}^-(E)dE=\int_0^{E_c}N_{ct}(E)f_{ct}^-(E)dE \ . \tag{22}$$

Finally, μ_{de} is obtained by relating the $\mu\tau$ product and τ_R as follows:

$$\mu_{de}=(\mu\tau)_e/\tau_R \ . \tag{23}$$

In Fig. 7 the calculated τ_R and μ_{de} are shown as a function of N_d, together with the measured data on the a-Si:H samples in the annealed and light-degraded states, respectively. The lowest limit of the time resolution in our transient photocurrent measurement is 200 ns. The small signal transient photocurrent is measured under a strong dc bias light corresponding to $g=5\times10^{19}$ cm^{-3}s^{-1} (solid symbols) and 2.5×10^{21} cm^{-3}s^{-1} (open symbols), respectively. The modulated beam (probe) has an intensity about a factor of 10 weaker than the bias beam. This condition enables us to approximate the photocurrent decay as a single exponential function before it decreases down to about 20% of its initial value.

As one can find in this figure, the agreement between the calculated and measured data for the annealed state is quite satisfactory. First, the calculated τ_R decreases from 10 μs to 3 ns when N_d increases from 10^{15} to 10^{19} cm^{-3} for the case of $g=5\times10^{19}$ cm^{-3}s^{-1}, which can be attributed to the decrease of τ_e. Second, τ_R is more sensitive to g when compared to $(\mu\tau)_e$, especially at high N_d.

The calculated μ_{de} shows a slight decrease from about 0.25 to 0.1 cm^{2}V^{-1}s^{-1} in the case of $g=5\times10^{19}$ cm^{-3}s^{-1} when N_d changes four orders of magnitude, in qualitative agreement with the measured data. Such a small change in μ_{de} is also consistent with published results which showed no observable change of electron drift mobility after light degradation.[44,45] In addition, the calculated μ_{de} increases with g. The enhancement of drift mobility by optical bias has been observed by many researchers[46–48] and interpreted qualitatively in terms of either the quasi-Fermi-level shift or defect relaxation model.[48] Here we want to give a simple explanation for the phenomenon based on $f_{ct}^-(E)$. As discussed above, most of the CBT states are trap states. Therefore, we can neglect the recombination term (R_3) and the hole reemission term (R_4) in these states. According to Eq. (8), the ratio of $N_{ct}^-(E)$ to n_f can be simplified to

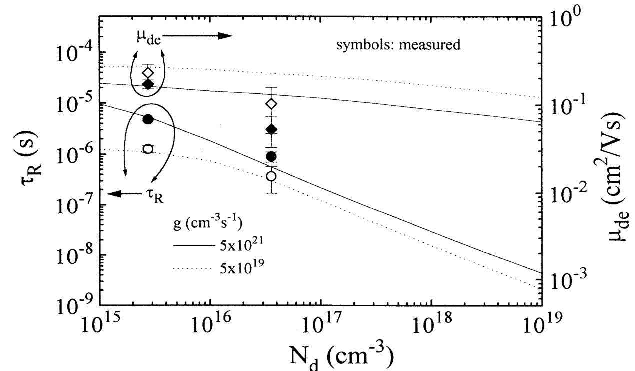

FIG. 7. The simulated τ_R and μ_{de} as a function of N_d for two generation rates. The symbols are the measured τ_R (circles) and μ_{de} (diamond) at $g\approx5\times10^{19}$ (solid) and 2.5×10^{21} cm^{-3}s^{-1} (open).

$$\frac{N_{ct}^{-}(E)}{n_f}=\frac{N_{ct}(E)f_{ct}^{-}(E)}{n_f}=\frac{c_1N_{ct}(E)}{ve^{-(E_c-E)/k_BT}+c_1n_f} . \quad (24)$$

The above equation implies that the increase of n_f by applying high g reduces the ratio $N_{ct}^{-}(E)/n_f$, especially for the deep trap states for which $ve^{-(E_c-E)/k_BT}<c_1n_f$. As a result, μ_{de} increases. This also explains the stronger effect of g on τ_R than on $(\mu\tau)_e$, because apart from the reduction of τ_e, the increase of g gives rise to an additional reduction of the ratio N_t/n_f. The same argument can also be applied to the slight decrease of μ_{de} with N_d, since n_f decreases with N_d; therefore, it slightly increases the ratio N_t/n_f.

As one can notice in Fig. 7, the measured μ_{de} in the light-degraded state deviates markedly from the calculation data. The measured value is about a factor of 4 lower then the calculated one. Here we tentatively attribute this discrepancy to the change of the DOS structure in the deep CBT states after degradation. Our simulation assumes the same single exponential function for the CBT states in the annealed and degraded states. As shown in Fig. 4 the peak position of $N_{ct}^{-}(E)$ shifts away from the band edge with N_d. Since the ratio of N_t/n_f is strongly dependent on the DOS structure, certainly the difference of the assumed DOS structure from the real one can give rise to some discrepancy.

B. Effect of the temperature

So far we have simulated the transport parameters at a constant temperature of 300 K. Temperature is a critical quantity determining the transport mechanism. For example, at low temperatures hopping transport via localized states becomes the dominant process. The multiple-trapping model used in this work is valid only above certain temperatures.[17] On the other hand, even in the framework of the multiple-trapping model, T strongly affects the reemission rate, which in return determines the net recombination rates at different localized states, especially those in the band tails. Therefore, in this section we want to simulate the temperature dependence of $\mu\tau$ products, τ_R and μ_{de}, and to test the validity of our simulation model in the temperature range between 150 and 450 K.

In Fig. 8 the calculated $\mu\tau$ products are shown as functions of $1/T$ for $E_a=0.8$ and 0.6 eV. The results are compared with our experimental data shown by the symbols in the figure. The measurements were done on an undoped a-Si:H sample in a cryostat, which enables us to change the temperature from 110 to 350 K. Again, $(\mu\tau)_e$ is evaluated from $\sigma_{\rm pc}$ and $(\mu\tau)_h$ from $L_{\rm amb}$.

As a first trial, we changed just the temperature, and performed the simulations with temperature-independent parameters as listed in Tables I and II. The overall tendencies of the T dependence of both $(\mu\tau)_e$ and $(\mu\tau)_h$ coincide with the experimental results; that is, both of them increase with T. But $(\mu\tau)_h$ is more sensitive to T than $(\mu\tau)_e$ in the case of undoped material.

The Fermi-level position strongly affects the tempera-

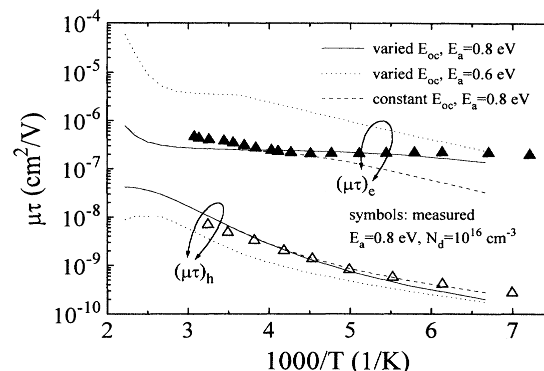

FIG. 8. The simulated $\mu\tau$ products as a function of $1/T$ for two values of E_v. The symbols are measured data at $g\approx5\times10^{19}$ $\mathrm{cm^{-3}\,s^{-1}}$. The dashed line is obtained with constant E_{oc}, and the other two with temperature dependent E_{oc}.

ture dependence of the $\mu\tau$ products. As E_f shifts to E_c, on the one hand, $(\mu\tau)_e$ increases in contrast to the decrease of $(\mu\tau)_h$, which can be attributed to the anticorrelated effect of the Fermi-level position on the $\mu\tau$ products.[49–51] On the other hand, at low temperatures the $\mu\tau$ products become insensitive to E_f and approach the same values. They are, for example, about $10^{-7}\ \mathrm{cm^2\,V^{-1}}$ for $(\mu\tau)_e$ and $2\times10^{-10}\ \mathrm{cm^2\,V^{-1}}$ for $(\mu\tau)_h$. But at high temperatures, the $\mu\tau$ products are strongly dependent on E_f. $(\mu\tau)_e$ shows a strong T dependence when E_f shifts toward E_c, consistent with experimental findings.[41]

The quantitative agreement between the simulated and measured $(\mu\tau)_h$ is quite satisfactory. However, the calculated $(\mu\tau)_e$ (dashed line) with temperature-independent simulation parameters shows a poor fit to the measured data. In particular, the deviation between them increases systematically with decreasing temperature. As will be seen below, the agreement between the simulated and measured τ_R becomes even worse in this case. The capture cross sections might change with T, but we think that the change of the DOS structures with T is the main factor leading to the discrepancy.

Aljishi *et al.* have measured E_{oc} and E_{ov} as functions of T by means of photoelectron yield spectroscopy in doped and undoped a-Si:H samples.[52] They found that both the DOS distributions of the CBT and VBT states are purely exponential functions of energy. Above room temperature E_{oc} increases almost linearly with T. For example, for undoped a-Si:H, E_{oc} is about 30 meV at 300 K and 50 meV at 500 K, respectively. Below room temperature E_{oc} shows a weaker T dependence. In contrast to E_{oc}, E_{ov} is not strongly affected by T. Aljishi *et al.* interpreted the results in terms of thermal disorder. Based on their results, for simplicity, we assume a T-independent E_{ov}, but E_{oc} changes as a linear function of T with two different slopes in different T ranges. Then we recalculated the $\mu\tau$ products. As shown in the figure, the agreement between the recalculated (solid line) and the mea-

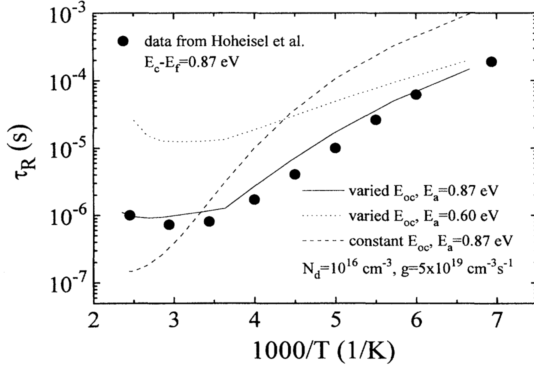

FIG. 9. The simulated response τ_R as a function of $1/T$ for two values of E_a. The symbols are experimental data published in Ref. 41.

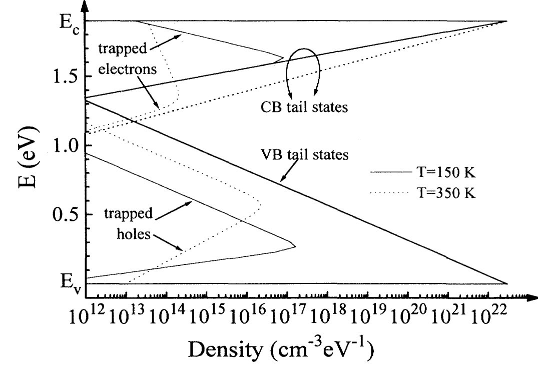

FIG. 11. The distribution of electrons and holes trapped in the CBT and VBT states at two different temperatures.

sured $(\mu\tau)_e$ is greatly improved. The best fit is reached with $E_{oc}=6+0.08T$ meV, when $T\geq 275$ K, and $E_{oc}=18.2+0.032T$ meV when $T<275$ K.

As in Sec. III B, we calculate τ_R and μ_{de} as functions of T. We have not yet measured τ_R and μ_{de} systematically at different T. Therefore, we took the published experimental results from Hoheisel and Fuhs[41] for comparison. The undoped *a*-Si:H sample has an E_a of 0.87 eV. As shown in Figs. 9 and 10, τ_R increases with decreasing T; however, μ_{de} decreases. As shown in Fig. 11, at low T there are more electrons trapped in the tail states than at high T, because carriers trapped in tail states at low T have less of a probability of being reemitted back to extended states. Therefore, the ratio of N_t to n_f increases at low T, which leads to the increase of τ_R and the decrease of μ_{de} according to Eqs. (21) and (23).

It is clear in Figs. 9 and 10 that the simulated τ_R and μ_{de} (dashed lines) using T-independent E_{oc} do not quantitatively fit the measured data. For example, the calculated τ_R is much larger than the measured one at low temperatures. In reverse, at higher temperatures the calculated τ_R becomes smaller than the measured one. We recall that τ_R and μ_{de} are directly related to the trapped electron density, which depends on the density of the CBT states. Therefore, the fact gives us a clue that the assumed density of the CBT states is too high at low T, and too low at high T for the simulation. This is evidence that the density of the tail state must increase with temperature. As done for the $\mu\tau$ products, we recalculated τ_R and μ_{de} by introducing a T-dependent E_{oc}. As one can see in Figs. 9 and 10, the recalculated curves (solid lines) fit to the measured data quite well.

Consistent with experimental findings,[41,43] the Fermi-level position strongly affects τ_R, as shown in Fig. 9. This can be attributed to the increase of the recombination lifetime of electrons when E_f is close to E_c. However, τ_R at low T is less sensitive to E_f than at high T. This is because at low temperatures the thermally excited carriers do not affect the occupation functions in the different gap states as strongly as at high temperatures.

On the other hand, μ_{de} is slightly enhanced when E_f moves toward E_c, as shown in Fig. 10. This means that the ratio N_t to n_f is not affected significantly by E_f if the DOS structure of the band tail states does not change. In

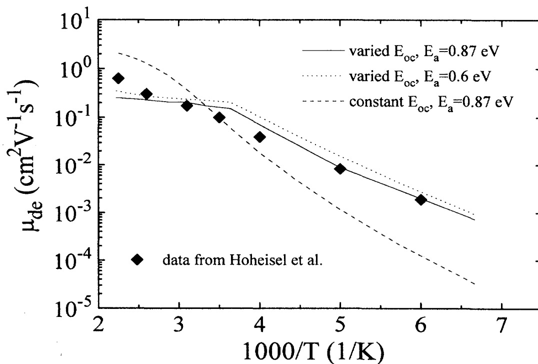

FIG. 10. The simulated μ_{de} as a function of $1/T$ with two E_a. The symbols are from Ref. 41.

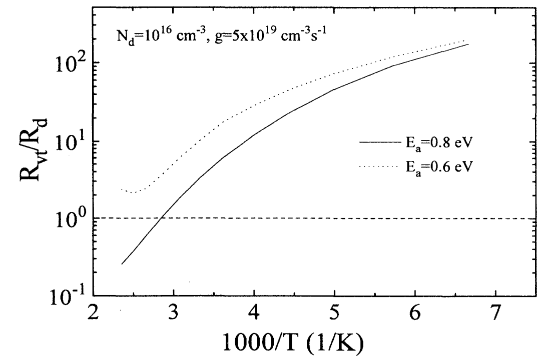

FIG. 12. The ratio of the net recombination rate via the VBT states to that at the defect states as a function of $1/T$.

the literature, one usually finds that μ_{de} decreases slightly with doping.[31,41] This discrepancy in our calculation can be easily ascribed to the change of the DOS structures with doping.[52]

Zhou and Elliott[53] found that, after intense light soaking at room temperature, the high-temperature photoconductivity decreases by more than one order of magnitude, but the low-temperature photoconductivity remains unchanged. These results mean that the recombination lifetime of free electrons at low temperatures is independent of the defect density. This again demonstrates the importance of the band-tail states on the recombination process. Figure 12 shows the ratio of R_{vt} to R_d as a function of T. It is clear that at low temperatures the recombination via the tail states entirely dominates the carrier recombination because at low T trapped carriers in the tail states have a very high probability to recombine before they are thermally reemitted back to the extended states.

IV. CONCLUSION

In summary, based on Shockley-Read-Hall statistics we have simulated the $\mu\tau$ products of electrons and holes, the response time of the photocurrent, and the electron drift mobility in a-Si:H as functions of dangling-bond density and temperature. We considered all possible recombination and reemission paths which may take place between extended and band tails or defect states. The simulated results are in good agreement with the experimental findings. The main conclusions are the following.

(a) $(\mu\tau)_e$ and $(\mu\tau)_h$ show an asymmetric dependence on N_d. $(\mu\tau)_h$ is insensitive to N_d in contrast to $(\mu\tau)_e$ in the low-N_d region. The asymmetric N_d dependence can be attributed to the inherent asymmetry between the valence- and conduction-band-tail states in a-Si:H.

(b) τ_R decreases substantially with N_d, but μ_{de} is only slightly affected by N_d. This means that the ratio of trapped to free-electron density is not significantly changed by N_d.

(c) The $\mu\tau$ products and μ_{de} increase with increasing T, whereas τ_R decreases. In undoped samples $(\mu\tau)_h$ shows a stronger T dependence than $(\mu\tau)_e$, which again can be attributed to the asymmetry between the two types of the tail states. The increase of the $\mu\tau$ products with T is explained in terms of the decrease of recombination rates in the tail states. The decrease of τ_R and increase of μ_{de} with T are mainly caused by the increase of the thermal reemission of trapped carriers in the tail states, which reduces the ratio of N_t/n_f.

(d) From the simulation we conclude that the characteristic energies of the tail states increase linearly with T. At low temperatures the T dependence of E_{oc} is weaker than at high temperatures.

(e) As a whole, both the recombination in the tails and the defect states must be considered in order to understand the recombination processes in a-Si:H. Recombination via the tail states is a predominant recombination path in the low-N_d range. In reverse, recombination in the defect states dominates the carrier recombination process only for high values of N_d. The transition from tail-state-dominated to defect-state-dominated recombination processes depends strongly on the defect density, the generation rate, the Fermi-level position, and the temperature.

ACKNOWLEDGMENTS

The work was partially supported by the Deutsche Forschungsgemeinschaft DFG. One of the authors (F.W.) would like to thank the Commission of the European Communities for financial support through the EU Programme "Human Capital & Mobility."

APPENDIX A: OCCUPATION FUNCTION OF THE VBT STATES

The four possible reactions occurring in a VBT state of energy E are the following, with the rates $R_5(E)$ to $R_8(E)$:

$$N_{vt}^0(E)+h\rightarrow N_{vt}^+(E),\quad R_5(E)=c_3p_fN_{vt}^0(E)\ , \tag{A1}$$

$$N_{vt}^+(E)+e\rightarrow N_{vt}^0(E),\quad R_6(E)=c_4n_fN_{vt}^+(E)\ , \tag{A2}$$

$$N_{vt}^+(E)\rightarrow N_{vt}^0(E)+h,\quad R_7(E)=\nu e^{-E/k_BT}N_{vt}^+(E)\ , \tag{A3}$$

$$N_{vt}^0(E)\rightarrow N_{vt}^+(E)+e\ ,\quad R_8(E)=\nu e^{-(E_c-E)/k_BT}N_{vt}0(E)\ , \tag{A4}$$

where $R_5(E)$ means trapping of free holes into the neutral VBT states. $R_6(E)$ is the capture of electrons by the positively charged VBT states and subsequent recombination. $R_7(E)$ is the thermal reemission of trapped holes back to the valence band. $R_8(E)$ is the thermal emission of electrons from the neutral VBT states to the conduction band. $N_{vt}^0(E)$ and $N_{vt}^+(E)$ are the density of the neutral and the positively charged VBT states. $c_3=\nu s_{voh}$ (s_{voh} is the capture cross section of the neutral VBT states for free holes). $c_4=\nu s_{vpe}$ (s_{vpe} is the capture cross section of the positively charged VBT states for free electrons). In the steady state,

$$\frac{dN_{vt}^0(E)}{dt}=-\frac{dN_{vt}^+(E)}{dt}=R_6(E)+R_7(E)-R_5(E)-R_8(E)=0\ . \tag{A5}$$

Because $N_{vt}(E)=N_{vt}^+(E)+N_{vt}^0(E)$, one can obtain $f_{vt}^+(E)$ [Eq. (10)].

APPENDIX B: OCCUPATION FUNCTION OF THE DEFECT STATES

As shown in Fig. 2, there are the following eight reactions which may take place in the defect states with the rates R_9 to R_{16}:

$$D^-\rightarrow D^0+e\ ,\quad R_9(E_d+U)=\nu e^{-(E_c-E_d-U)/k_BT}N_d^-(E_d+U)\ , \tag{B1}$$

$$D^++e\rightarrow D^0,\quad R_{10}(E_d)=c_5n_fN_d^+(E_d)\ , \tag{B2}$$

$$D^0+e\rightarrow D^-,\quad R_{11}(E_d)=c_6 n_f N_d^0(E_d)\ , \tag{B3}$$

$$D^0\rightarrow D^+ + e,\quad R_{12}(E_d)=\nu e^{-(E_c-E_d)/k_BT} N_d^0(E_d)\ , \tag{B4}$$

$$D^-+h\rightarrow D^0,\quad R_{13}(E_d+U)=c_7 p_f N_d^-(E_d+U)\ , \tag{B5}$$

$$D^+\rightarrow D^0+h,\quad R_{14}(E_d)=\nu e^{-E_d/k_BT} N_d^+(E_d)\ , \tag{B6}$$

$$D^0\rightarrow D^-+h,\quad R_{15}(E_d)=\nu e^{-E_d/k_BT} N_d^0(E_d)\ , \tag{B7}$$

$$D^0+h\rightarrow D^+,\quad R_{16}(E_d)=c_8 p_f N_d^0(E_d)\ , \tag{B8}$$

where $R_9(E_d+U)$ denotes the thermal reemission of electrons in D^- states back to the conduction band. $R_{10}(E_d)$ is the recombination of holes in D^+ states with free electrons. $R_{11}(E_d)$ is the trapping of free electrons into D^0 states. $R_{12}(E_d)$ is the thermal emission of electrons from D^0 states to the conduction band. $R_{13}(E_d+U)$ is the recombination of electrons in D^- states with free holes. $R_{14}(E_d)$ is the thermal reemission of holes in D^+ states back to the valence band. $R_{15}(E_d)$ is the thermal emission of holes from D^0 states to the valence band. $R_{16}(E_d)$ is the trapping of free holes into D^0 states. $N_d^-(E_d+U)$, $N_d^+(E_d)$, and $N_d^0(E_d)$ are the densities of D^-, D^+, and D^0 states, respectively. The coefficients are $c_5=\upsilon s_{dpe}$ (s_{dpe} is the capture cross section of D^+ states for free electrons). $c_6=\upsilon s_{doe}$ (s_{doe} is the capture cross section of D^0 states for free electrons), $c_7=\upsilon s_{dnh}$ (s_{dnh} is the capture cross section of D^- states for free holes), and $c_8=\upsilon s_{doh}$ (s_{doh} is the capture cross section of D^0 states for free holes).

The steady-state condition requires that in the defect states

$$\frac{dN_d^-(E_d+U)}{dt}=\frac{dN_d^+(E_d)}{dt}=\frac{dN_d^0(E_d)}{dt}=0\ . \tag{B9}$$

For the D^+ states, one has

$$\frac{dN_d^+(E_d)}{dt}=R_{16}(E_d)+R_{12}(E_d)-R_{10}(E_d)-R_{14}(E_d)=0\ . \tag{B10}$$

Insertion of $R_{16}(E_d)$, $R_{12}(E_d)$, $R_{10}(E_d)$, and $R_{14}(E_d)$ into the above equation yields

$$N_d^+(E_d)=\frac{c_8 p_f+\nu e^{-(E_c-E_d)/k_BT}}{c_5 n_f+\nu e^{-E_d/k_BT}} N_d^0(E_d)\ . \tag{B11}$$

In the same way for $N_d^-(E_d+U)$, we find

$$\frac{dN_d^-(E_d+U)}{dt}=R_{15}(E_d)+R_{11}(E_d)-R_9(E_d+U)-R_{13}(E_d+U)\ . \tag{B12}$$

Therefore, $N_d^-(E_d+U)$ can be expressed in terms of $N_d^0(E_d)$ by

$$N_d^-(E_d+U)=\frac{\nu e^{-E_d/k_BT}+c_6 n_f}{\nu e^{-(E_c-E_d-U)/k_BT}+c_7 p_f} N_d^0(E_d)\ . \tag{B13}$$

Since the total dangling-bond density is $N_d=N_d^0(E_d)+N_d^+(E_d)+N_d^-(E_d+U)$, we obtain

$$N_d=\left[1+\frac{c_8 p_f+\nu e^{-(E_c-E_d)/k_BT}}{c_5 n_f+\nu e^{-E_d/k_BT}}+\frac{\nu e^{-E_d/k_BT}+c_6 n_f}{\nu e^{-(E_c-E_d-U)/k_BT}+c_7 p_f}\right] N_d^0(E_d)\ . \tag{B14}$$

Therefore, we can obtain f_d^0, f_d^-, and f_d^+ as shown by Eqs. (11)–(13).

[1]R. A. Street, Philos. Mag. B **46**, 273 (1982).

[2]H. Dersch, L. Schweitzer, and J. Stuke, Phys. Rev. B **28**, 4678 (1983).

[3]S. P. Hotaling, H. Antoniadis, and E. A. Schiff, J. Non-Cryst. Solids **114**, 420 (1989).

[4]J. H. Yoon, in *Amorphous Silicon Technology–1993,* edited by E. A. Schiff, M. J. Thompson, A. Madan, K. Tanaka, and P. G. LeComber, MRS Symposia Proceedings No. 297 (Materials Research Society, Pittsburgh, 1993), p. 455.

[5]N. Beck, N. Wrysch, E. Sauvain, and A. Shah, in *Amorphous Silicon Technology–1993* (Ref. 4), p. 479.

[6]J. Kočka, C. E. Nebel, and C. D. Abel, Philos. Mag. B **63**, 221 (1990).

[7]M. Hack, S. Guha, and M. Shur, Phys. Rev. B **30**, 6991 (1984).

[8]S. Lee, M. Gunes, C.R. Wronski, N. Maley, and M. Bennett, Appl. Phys. Lett. **59**, 1578 (1992).

[9]C. R. Wronski, R. M. Dawson, M. Gunes, Y. M. Li, and R. W. Collins, in *Amorphous Silicon Technology–1993* (Ref. 4), p. 443.

[10]L. Y. Yang, A. Catalano, R. R. Arya, and I. Balberg, Appl. Phys. Lett. **57**, 908 (1990).

[11]E. Sauvain, J. Hubin, A. Shah, and P. Pipoz, Philos. Mag. Lett. **63**, 327 (1991).

[12]F. Wang and R. Schwarz, J. Appl. Phys. **71**, 791 (1992).

[13]G. Conte, G. Fameli, G. Nobile, A. Rubino, E. Terzini, F. Villani, D. Caputo, G. de Cesare, F. Irrera, F. Palma, and M. C. Rossi, in *Materials Interactions Relevant to the Pulp, Paper, and Wood Industries,* edited by D. F. Caulfield, J. D. Pasaretti, and S. F. Subczynski, MRS Symposia Proceedings No. 197 (Materials Research Society, Pittsburgh, 1993), p. 485.

[14]W. Shockley and W. T. Read, Phys. Rev. **87**, 835 (1952).

[15]J. G. Simmons and G. W. Taylor, Phys. Rev. B **4**, 502 (1971).

[16]J. G. Simmons and G. W. Taylor, J. Non-Cryst. Solids **8-10**, 947 (1972).

[17]T. Tiedje, in *Hydrogenated Amorphous Silicon, Part B: Optical Properties,* edited by J. I. Pankove, Semiconductors and Semimetals Vol. 21 (Academic, New York, 1984), p. 207.

[18]F. Vaillant and D. Jousse, Phys. Rev. B **34**, 4088 (1986).

[19]J. Hubin, A. Shah, and E. Sauvain, Philos. Mag. Lett. **66**, 115 (1992).

[20]E. Morgado, Philos. Mag. B **63**, 529 (1991).

[21]R. H. Bube and D. Redfield, J. Appl. Phys. **66**, 3074 (1989).

[22]I. Sakata and Y. Hayashi, Appl. Phys. A **37**, 153 (1985).
[23]C. D. Abel and G. H. Bauer, in *Light Emission From Silicon,* edited by S. S. Iyer, R. T. Collins, and L. T. Canham, MRS Symposia Proceedings No. 256 (Materials Research Society, Pittsburgh, 1992), p. 705.
[24]N. Hata and S. Wagner, J. Appl. Phys. **71**, 2857 (1992).
[25]G. Amato, F. Giorgis, and R. Spagnolo, J. Appl. Phys. **71**, 3479 (1992).
[26]C. R. Wronski, S. Lee, M. Hicks, and S. Kumar, Phys. Rev. Lett. **63**, 1420 (1989).
[27]J. Kočka, M. Vaněček, and A. Třiska, in *Amorphous Silicon and Related Materials A,* edited by H. Fritzsche (World Scientific, Singapore, 1989), p. 297.
[28]I. Hirabayashi, K. Winer, and L. Ley, J. Non-Cryst. Solids **97/98**, 87 (1987).
[29]K. Winer, Phys. Rev. Lett. **63**, 1487 (1989).
[30]J. M. Marshall, R. A. Street, M. J. Thompson, and W. B. Jackson, Philos. Mag. B **57**, 387 (1988).
[31]W. E. Spear, in *Amorphous Silicon and Related Materials B,* edited by H. Fritzsche (World Scientific, Singapore, 1989), p. 721.
[32]A. Rose, *Concepts in Photoconductivity and Allied Problems* (Wiley Interscience, New York, 1963).
[33]D. Ritter, E. Zeldov, and K. Weiser, Appl. Phys. Lett. **49**, 791 (1986).
[34]I. Balberg, in *Amorphous Silicon Technology–1992,* edited by M. J. Thompson, Y. Hamakawa, P. G. LeComber, A. Madan, and E. A. Schiff, MRS Symposia Proceeding No. 258 (Materials Research Society, Pittsburgh, 1992), p. 693.
[35]M. Vaněček, J. Kočka, J. Stuchlík, Z. Kozesík, and A. Třiska, Solar Energy Mater. **8**, 411 (1983).
[36]D. L. Staebler and C. R. Wronski, Appl. Phys. Lett. **31**, 292 (1972).
[37]M. Hack and M. Shur, J. Appl. Phys. **55**, 2967 (1984).
[38]M. Haridim, M. Zelikson, and K. Weiser, Phys. Rev. B **49**, 13 394 (1993).
[39]C. R. Wronski and R. E. Daniel, Phys. Rev. B **23**, 794 (1981).
[40]R. Pandya and E. A. Schiff, Philos. Mag. B **52**, 1075 (1985).
[41]B. Hoheisel and W. Fuhs, Philos. Mag. B **57**, 411 (1988).
[42]E. Zeldov and K. Weiser, Phys. Rev. Lett. **53**, 1012 (1984).
[43]R. Schwarz, F. Wang, S. Grebner, T. Fischer, S. Koynov, V. Chu, P. Brogueira, and J. Conde, J. Non-Cryst. Solids **164/166**, 477 (1993).
[44]C. E. Nebel and G. H. Bauer, J. Non-Cryst. Solids **114**, 600 (1989).
[45]Q. Wang, H. Antoniadis, and E. A. Schiff, Appl. Phys. Lett. **60**, 2791 (1992).
[46]R. Pandya, E. A. Schiff, and K. A. Conrad, J. Non-Cryst. Solids **66**, 193 (1984).
[47]H. Oheda, J. Appl. Phys. **73**, 3396 (1992).
[48]D. Han, D. C. Melcher, E. A. Schiff, and M. Silver, Phys. Rev. B **48**, 8658 (1993).
[49]T. Kagawa, N. Matsumoto, and K. Kumabe, Phys. Rev. B **28**, 4570 (1983).
[50]R. Schwarz, F. Wang, and M. Reissner, Appl. Phys. Lett. **63**, 1083 (1993).
[51]I. Balberg and Y. Lubianiker, Phys. Rev. B **48**, 8709 (1993).
[52]S. Aljishi, J. D. Cohen, S. Jin, and L. Ley, Phys. Rev. Lett. **64**, 2811 (1990).
[53]J. H. Zhou and S. R. Elliott, Philos. Mag. B **66**, 801 (1992).

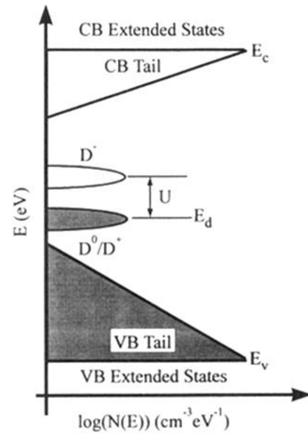

FIG. 1. Model of the density-of-states distribution in the mobility gap used for the simulation.